PERGAMON

International Journal of Solids and Structures 38 (2001) 2427–2451

INTERNATIONAL JOURNAL OF SOLIDS and STRUCTURES

www.elsevier.com/locate/ijsolstr

Anisotropic behaviour of porous, ductile media

Stefano Mariani, Alberto Corigliano *

Department of Structural Engineering, Politecnico di Milano, Piazza L. da Vinci 32, 20133 Milano, Italy

Received 15 November 1999; in revised form 21 April 2000

Abstract

An orthotropic constitutive model for porous, ductile media is developed, which is centred on the micromechanical analysis of a cylindrical representative volume element (RVE) with elliptic cross-section containing a coaxial and confocal elliptic-cylindrical cavity. The constitutive model is obtained in the case of a rigid ideally plastic behaviour of the matrix material, whose yield condition obeys J_2 flow theory of plasticity with an associated flow rule. The following condition is assumed throughout: the longitudinal axis of the hollow cylindrical RVE is a principal direction of the macroscopic strain rate and stress tensors. Cases for which the principal directions of the macroscopic strain rate tensor in the RVE cross-section plane are aligned or rotated with respect to the ellipse axes are both considered. The constitutive behaviour is characterized by the homogenized yield domain in the macroscopic stress tensor space, by associated flow rules for the plastic components of the macroscopic strain rate tensor and by the evolution laws for the internal state variables. These are the void volume fraction, already appearing in Gurson's model, the aspect ratio of the cavity and its orientation in the RVE cross-section plane, assuming that during the deformation process, the void retains an elliptic shape. The theoretical results are compared with finite element computations of the RVE strength at plastic collapse to assess the capability of the model to describe the actual micromechanical response to the applied boundary conditions.

Keywords: Micro-mechanics; Limit analysis; Homogenization; Anisotropic composite materials

1. Introduction

During the last two decades, the micromechanical description of ductile crack growth has received much attention. Starting from the pioneering works of McClintock (1968) and Rice and Tracey (1969) on isolated cylindrical and spherical voids in viscous and plastic materials, respectively, with strain-hardening properties and rigid perfectly plastic media, models for the description of the damage process leading to ductile fracture have been developed in order to take into account its actual micromechanical features.

Gurson's constitutive model (Gurson, 1977), which phenomenologically describes at the macroscale the degradation of the material strength properties due to the microscopic void growth to coalescence, has set the bases for numerical simulations of crack growth processes in ductile media (Xia et al., 1995).

* Corresponding author. Tel.: +39-2-2399-4244; fax: +39-2-2399-4220.
E-mail addresses: mariani@stru.polimi.it (S. Mariani), coriglia@stru.polimi.it (A. Corigliano).

0020-7683/01/$ - see front matter
PII: S0020-7683(00)00190-6

Alternative descriptions of ductile fracture processes have been developed, within the framework of continuum damage mechanics, e.g. by Lemaitre (1992) and Rousselier (1981). This latter approach does not constitute a reference for the study presented in this paper, where attention is focused on the homogenized properties of a single representative volume element (RVE) that locally describes in an average (or smeared) fashion the actual distribution of microvoids within the matrix material.

From an experimental viewpoint, results have shown that ductile fracture is triggered by the presence of inclusions within the plastic matrix material (Goods and Brown, 1979; Speich and Spitzig, 1982). These inclusions, or second-phase particles, are usually characterized by elastic and strength properties different from those of the matrix material. The decohesion at the particle–matrix interface and the particle rupture are the micromechanical phenomena of crack initiation.

The subsequent macroscopic crack growth is governed by the process of void growth to coalescence, and is strongly influenced by the spatial distribution of the inclusions within the matrix. During the first stage of the microvoids growth, the largest inclusions, according to some sort of weakest-link process, play the main role. In the subsequent phase, microvoids can be nucleated at the interface between matrix and smaller inclusions giving rise to phenomena governed by failure mechanisms at different size scales (Faleskog and Shih, 1997). The phenomenological description of the material behaviour at a length scale comparable to those of the specimen geometry and of the variation of the applied loading conditions thus needs to take into account the microstructure of the solid.

Porous, ductile media can be studied at the micromechanical level as two-phase composites, the first phase being the rigid ideally plastic metal matrix and the second one, the cavity (with vanishing strength properties) which is surrounded by the matrix. In order to obtain the overall (or effective, homogenized) constitutive behaviour of the porous, ductile solid, that is of a void-containing metal matrix, homogenization techniques are required. These techniques must be able to handle the nonlinear response of the matrix material and the spatial arrangement of the voids.

Gurson's model, which is a micromechanics-based constitutive description of the material behaviour in the fracture process zone during ductile tearing processes, has been obtained from the study of a cavity contained in a finite-dimensions RVE. This model, which describes the void growth process, is not able to follow the material response during the final coalescence process that drastically reduces the local load-carrying capacity. Various modifications to the original yield condition and evolution law for the void volume fraction (or porosity) have been proposed in order to improve the agreement between experimental and numerical results obtained through this model for strain localization and subsequent fracture processes (Tvergaard, 1990).

Recently, the effects of anisotropic microstructures on the effective behaviour of two-phase composites have been studied. Since during finite-deformation loading processes the microstructural geometry can be largely distorted by plastic strains, account has to be taken of this aspect to accurately describe the actual response of porous media under general loading conditions.

Under axisymmetric loadings, effective properties of metals containing particulate spheroidal voids or inclusions have been obtained by Mear and coworkers for an ideally plastic matrix behaviour (Lee and Mear, 1991) and for a power-law matrix material under steady-state creeping conditions (Lee and Mear, 1992a; Yee and Mear, 1996). A variational characterization of the nonlinear behaviour of porous media at finite-strains has been derived by Ponte Castañeda and coworkers under the assumption of particulate ellipsoidal inclusions distributed within the matrix with an ellipsoidal symmetry (Castañeda and Zaidman, 1994; Kailasam et al., 1997a,b; Kailasam and Castañeda, 1998). Ellipsoidal microstructures have been also analyzed by Gologanu et al. (1993, 1994): under axisymmetric loading conditions approximate homogenized yield criteria and evolution laws for the microstructure, which is assumed to retain an ellipsoidal shape throughout the whole deformation process, were proposed for a rigid ideally plastic matrix material.

In this paper, different anisotropic microstructure and loading conditions are considered. As far as the RVE geometry is concerned, the analysis is carried out for a cylindrical volume with an elliptic cross-section

containing a coaxial confocal elliptic-cylindrical cavity. This RVE geometry allows to take into account effects due to variations of the RVE cross-section geometry under the constraint that the longitudinal RVE axis is a principal direction of the overall stress and strain rate tensors. In order to assess the influence of the void cross-section geometry on the homogenized behaviour of porous-ductile solids, axisymmetric boundary conditions are relaxed. The considered boundary conditions allow the void to evolve not only in volume but also in shape and orientation with respect to a fixed reference frame.

This study set the bases for the formulation of constitutive models for anisotropic porous, ductile media, whose behaviour is described by means of an instantaneous effective yield condition, associated flow rules for the plastic components of the macroscopic strain-rate tensor and evolution laws for the internal state variables that are assumed to characterize the microstructural geometry.

To appraise the degree of accuracy of the proposed effective yield condition, a comparison is presented with finite element simulations of the plastic collapse mechanisms within the ideally plastic matrix material as obtained by applying the same loading conditions used to derive the analytical solution.

Results in this paper are reported as follows. In Section 2, Gurson's approach to obtain the effective mechanical properties of porous-ductile media is revised and discussed in the case of rigid ideally plastic matrix behaviour. In Section 3, the orthotropic microstructure is analyzed and estimates for the effective yield function as well as the evolution laws for the internal state variables that describe the microstructural geometry are derived. Section 4 concerns finite element computations of unit cell strength properties at fixed microstructure that are compared with the previously derived analytical results. Discussion and conclusions on the present study are finally presented in Section 5.

2. Review of Gurson's homogenization approach for porous media

The nonlinear effective behaviour of porous, ductile media can be obtained, as mentioned in the Section 1, by treating the porous material as a two-phase composite, the second phase (void) being characterized by vanishing strength properties.

In this section, the approach to obtain the overall mechanical properties of porous, plastic media introduced by Gurson (1977) on the basis of the variational analysis of multi-phase aggregates given by Bishop and Hill (1951) is briefly described in order to set the stage for its subsequent application in Section 3 to orthotropic materials.

Let us consider an RVE of a two-phase heterogeneous material. It is assumed that the composite possesses a finite microscale, with dimensions comparable to those of the inclusions, and a uniform microstructure only in a statistical sense, so that periodic boundary conditions (Taliercio, 1992; Suquet, 1996) are not dealt with in the analysis of the single RVE. Thus, as is common practice in treating non-homogeneous materials (Castañeda, 1996), bounds are obtained on the nonlinear overall properties of the composite.

Once the microstructure has been defined in terms of the void volume fraction and, eventually, higher order information has been gained by overall symmetries in the distribution of the cavities within the solid, the homogenized properties of the heterogeneous medium can be characterized in terms of average (or macroscopic) quantities over the RVE, namely in terms of the macroscopic strain rate $\dot{E}_{ij}$ and stress Σ_{ij} tensors, respectively defined as

$$\dot{E}_{ij} \equiv \frac{1}{V}\int_V \dot{\epsilon}_{ij}\,\mathrm{d}V, \quad \Sigma_{ij} \equiv \frac{1}{V}\int_V \sigma_{ij}\,\mathrm{d}V, \qquad i,j = 1,2,3, \tag{1}$$

where V is the RVE volume and $\dot{\epsilon}_{ij}$ and σ_{ij} are the local strain rate and stress tensors, respectively.

The overall response of the RVE is sought for a given linear velocity field on the outer boundary ∂V of the RVE:

$$v_i(\boldsymbol{x}) = \dot{E}_{ij}x_j \quad \text{on } \partial V, \tag{2}$$

$\boldsymbol{x}$ being the position vector in the RVE.

The nonlinear behaviour of the rigid perfectly plastic matrix material is assumed incompressible, with a yield condition $\phi(\sigma_{ij}) = 0$ described by means of J_2 flow theory of plasticity:

$$\phi(\sigma_{ij}) = \sigma_{\text{eq}} - \sigma_0 = \sqrt{\frac{3}{2}s_{ij}s_{ij}} - \sigma_0, \qquad s_{ij} = \sigma_{ij} - \frac{\sigma_{kk}}{3}\delta_{ij}, \tag{3}$$

where s_{ij} is the deviatoric stress tensor, σ_{eq}, the Mises effective stress, σ_{kk}, the stress tensor trace, δ_{ij}, the Kronecker delta, and σ_0, the uniaxial strength of the matrix material. An associated flow rule gives rise to

$$s_{ij} = \frac{\sqrt{\frac{2}{3}}\sigma_0}{\sqrt{\dot{\epsilon}_{kl}\dot{\epsilon}_{kl}}}\dot{\epsilon}_{ij}, \quad k,l = 1,2,3. \tag{4}$$

Now, let the macroscopic plastic dissipation be defined according to

$$\dot{W} \equiv \frac{1}{V}\int_V \dot{w}\,\mathrm{d}V = \frac{1}{V}\int_V \sigma_{ij}\dot{\varepsilon}_{ij}\,\mathrm{d}V = \frac{1}{V}\int_\Omega \sigma_{ij}\dot{\varepsilon}_{ij}\,\mathrm{d}V = \frac{\sigma_0}{V}\int_\Omega \dot{\varepsilon}_{\text{eq}}\,\mathrm{d}V, \tag{5}$$

where the local plastic dissipation $\dot{w}$ is the doubly contracted product of the microscopic stress and strain rate tensors, $\dot{\varepsilon}_{\text{eq}}$ is the Mises effective strain rate defined as $\dot{\varepsilon}_{\text{eq}} = \sqrt{\frac{2}{3}\dot{\varepsilon}_{ij}\dot{\varepsilon}_{ij}}$, $\dot{\varepsilon}_{ij}$ being a divergence-free strain rate field over the matrix volume Ω. In the Eq. (5), the integration is taken over the volume Ω of the rigid ideally plastic matrix due to the null strength properties of the void.

By means of the Bishop and Hill no-correlation postulate (Bishop and Hill, 1951), which assumes that no correlation exists between the components of the microscopic stress tensor σ_{ij} and the components of the velocity field v_i over any plane section of the RVE, the macroscopic plastic dissipation (5) can be expressed as

$$\dot{W} \equiv \frac{1}{V}\int_V \sigma_{ij}\dot{\varepsilon}_{ij}\,\mathrm{d}V = \Sigma_{ij}\dot{E}_{ij}. \tag{6}$$

It is worth emphasizing here that relation (6) does not follow immediately from definition (1) of the macroscopic strain rate and stress tensors and from the applied boundary conditions (2) as given by Hill's macrohomogeneity equality. In fact, this equality requires that the relation $v_i = \dot{E}_{ij}x_j$ (i.e. $\dot{\varepsilon}_{ij} = \dot{E}_{ij}$) holds locally within the whole RVE, $\dot{E}_{ij}$ being independent of the position vector $\boldsymbol{x}$; as it will be shown in the next section, results are here obtained for $\dot{\varepsilon}_{ij} \neq \dot{E}_{ij}$ and the no-correlation postulate needs to be introduced. Since the local associated J_2 yield condition fulfills convexity requirements at the microscale, a macroscopic maximum work principle can be deduced from the microscopic one and from the no-correlation postulate (Gurson, 1977). The effective yield function thus inherits the property of associativity of the local one for the matrix material (Maier and Drucker, 1973). An upper bound on the macroscopic stress tensor at yielding can be obtained, by exploiting the associativity of the macroscopic flow rule and Eq. (5), as

$$\Sigma_{ij} = \frac{\partial\dot{W}}{\partial\dot{E}_{ij}} = \frac{\sigma_0}{V}\int_\Omega \frac{\partial\dot{\varepsilon}_{\text{eq}}}{\partial\dot{E}_{ij}}\,\mathrm{d}V. \tag{7}$$

In Section 3, the above procedure is applied to obtain estimates of the effective RVE strength properties and evolution laws for the internal state variables that characterize the microstructural geometry. Within the present approach, the evolution laws can be obtained by studying the effects of the instantaneous plastic collapse mechanism, as governed by the boundary conditions (2), on the void shape, size and orientation.

Microstructure evolution, which has been recently shown to have a strong influence on the nonlinear behaviour of porous, ductile media at finite strains (Castañeda and Zaidman, 1994; Kailasam et al., 1997b), is studied in details in order to get insights into the actual void growth mechanisms. This aspect is specially important under quasi purely deviatoric states of stress for which the void volume fraction holds a nearly constant value (see below), thus freezing the overall softening behaviour of the homogenized void-containing material.

3. Effective mechanical properties of orthotropic porous, ductile media

Gurson's model is not able to reproduce softening effects at the macroscopic level induced by predominantly deviatoric stress fields. In such cases, the dilatancy predicted by an associated flow rule is almost zero, thus preventing the void volume growth and the relevant increase in the induced softening. In order to overcome problems related to the description of the microstructure in terms of the void volume fraction only, additional conditions for void nucleation from small scale second-phase particles have been introduced in the original Gurson's model (Chu and Needleman, 1980).

In this section, an alternative approach is presented. It rests on a more refined description of the microstructure, which is based on the void volume fraction and on the aspect ratio of the void in its transverse cross-section. In what follows, in order to simplify the analytical treatment, the microstructural geometry is characterized by means of a cylindrical RVE with an elliptic cross-section, containing a coaxial and confocal elliptic-cylindrical cavity (Fig. 1a). The considered ellipses can have the major axis either along x_2 or along x_1. The anisotropy of the RVE cross-section is described by the parameter c, defined as

$$c \equiv \frac{a_1^2 - b_1^2}{4} = \frac{a_2^2 - b_2^2}{4}, \tag{8}$$

where a_i and b_i $(i = 1, 2)$ are the semiaxis lengths aligned with the reference axes x_2 and x_1, respectively (Fig. 1). From Eq. (8) it follows that: $c > 0$ when the ellipse is as in Fig. 1b with the major axis along x_2 and a distance $e_2 = \sqrt{4c}$ between the origin of the reference frame and the foci of the ellipse; $c = 0$ when the ellipse reduces to a circle (Fig. 1c); $c < 0$ when the ellipse has its major axis along x_1 and a distance origin-foci $e_1 = \sqrt{-4c}$ (Fig. 1d).

By means of this model, an extension of the circular cylindrical Gurson's model is achieved (Gurson, 1977). Aim of this model is to take into account the anisotropy at the microstructural level induced by the shape and spatial arrangement of the voids as well as by plastic straining during external action increase.

This RVE geometry does not allow to fill the continuum without gaps or overlaps: the bounds on the RVE strength have thus to be intended as approximate estimates of the actual behaviour of the homogenized continuum.

Under generalized plane strain conditions, namely with a constant longitudinal strain rate in the whole RVE, the longitudinal shear strain rate components are assumed to be zero, both at the microscopic level within the matrix and at the macroscopic level. This assumption allows to take into account only four independent components of the macroscopic strain rate and stress tensors. Loading conditions on the RVE are represented by the prescribed uniform strain rates (2) on the outer boundary ∂V.

The internal state variables that define the orthotropic microstructure are the void volume fraction f, the void aspect ratio λ and the orientation of the void axes in the transverse cross-section with respect to a fixed global reference frame.

The porosity f is defined as the ratio between the void volume V_v and the whole RVE volume V:

$$f = \frac{V_v}{V} = \frac{a_1 b_1}{a_2 b_2}, \tag{9}$$

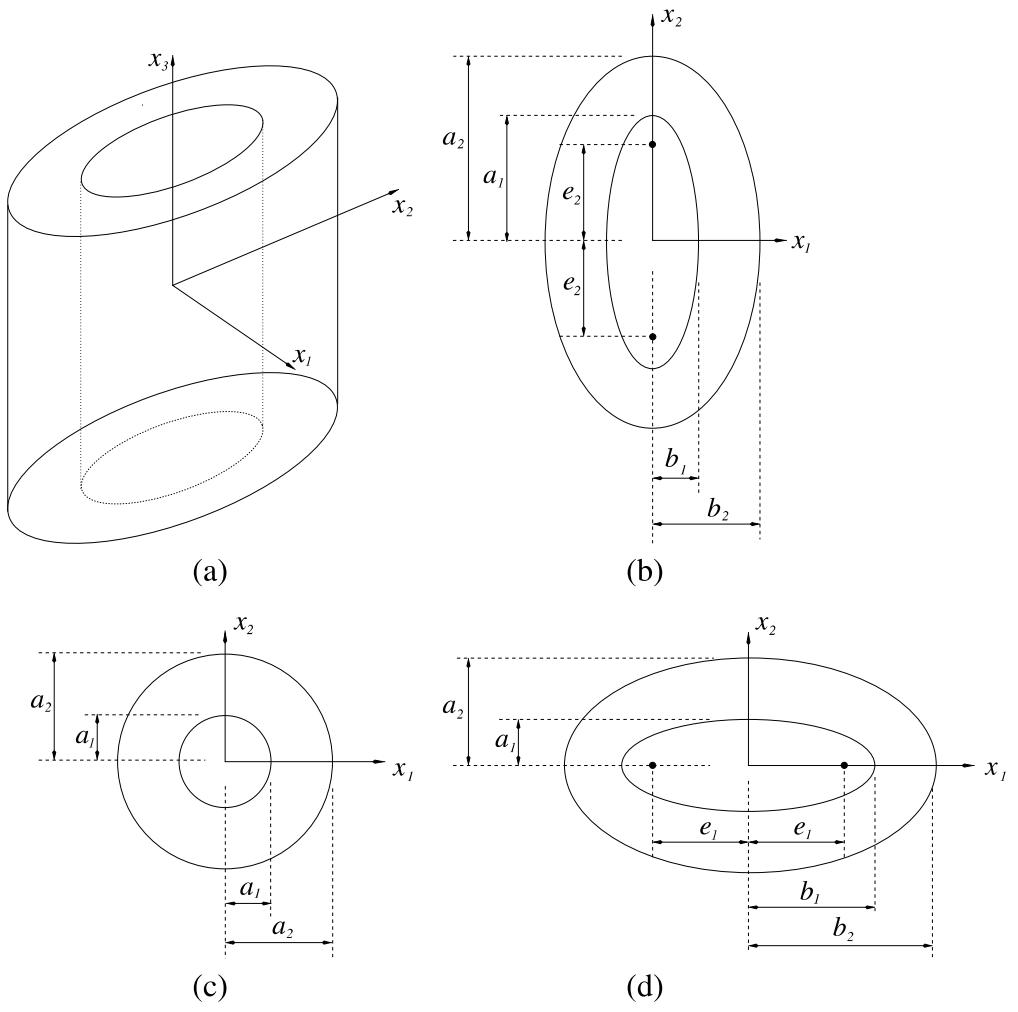

Fig. 1. Geometry of the orthotropic RVE.

where subscript 1 refers to quantities computed on the void surface while subscript 2 refers to quantities at the RVE external boundary.

The aspect ratio λ is defined as the ratio between the lengths of the ellipse axes aligned with the reference axes x_2 and x_1 at the cavity surface:

$$\lambda = \frac{a_1}{b_1}. \tag{10}$$

The orientation of the void axes is described by means of the angle between the local x_2 axis and the global X_2 one.

Eqs. (9) and (10) define the internal state variables f and λ in terms of a_1, b_1, a_2 and b_2. Assigning the RVE volume V, the porosity f, the aspect ratio λ and the longitudinal length L of the RVE, the values of the semiaxes lengths are

$$a_1 = \sqrt{\frac{f\lambda}{\pi}\frac{V}{L}}, \tag{11a}$$

$$b_1 = \sqrt{\frac{f}{\pi\lambda}\frac{V}{L}}, \tag{11b}$$

$$a_2 = \sqrt{\frac{\kappa_V}{\pi}\frac{V}{L}}, \tag{11c}$$

$$b_2 = \sqrt{\frac{1}{\pi\kappa_V}\frac{V}{L}}, \tag{11d}$$

where

$$\kappa_V \equiv \left(\frac{fV}{2}\frac{\lambda^2-1}{\lambda}\right) + \sqrt{1+\left(\frac{fV}{2}\frac{\lambda^2-1}{\lambda}\right)^2}. \tag{12}$$

In what follows, the effective mechanical properties of orthotropic porous, plastic solids are presented in terms of the instantaneous yield locus, which is a function of the matrix strength and of the current microstructure (here of the current porosity f and void aspect ratio λ), and in terms of the evolution laws for the internal state variables.

Notice that, as discussed in Section 2, associativity of the matrix material is preserved at the macroscale by the homogenized yield condition, so that the direction of macroscopic plastic straining coincides with the outward normal to the effective yield domain.

3.1. Upper bounds on the effective yield condition

Effective yield conditions for orthotropic porous media have to depend on the microstructure, namely on the void volume fraction and on the void aspect ratio, both in the presence and in the absence of a macroscopic shear straining in the RVE transverse cross-section.

An ad-hoc transformation of coordinates is needed in order to describe the RVE cross-section geometry in a simple way. A new coordinate mapping is introduced and used throughout; this mapping proves to be more suitable than the standard elliptic one (Lee and Mear, 1992b,c) for numerical calculations.

The upper bounds on the overall yield condition are then obtained with increasing degree of approximation.

3.1.1. Elliptic-cylindrical coordinates

Let the elliptic-cylindrical mapping be defined on the x_1–x_2 plane according to

$$\begin{cases} x_1 = (r - h(r))\sin\beta, \\ x_2 = (r + h(r))\cos\beta, \end{cases} \tag{13}$$

where, in order to simplify the computations, function h has been assumed to depend on the radial-like coordinate r only.

The orthonormal curvilinear coordinates (r, β) have to satisfy the orthogonality condition (Malvern, 1969)

$$\frac{\partial x_1}{\partial r}\frac{\partial x_1}{\partial \beta} + \frac{\partial x_2}{\partial r}\frac{\partial x_2}{\partial \beta} = \sin\beta\cos\beta\left\{\left(1 - \frac{\mathrm{d}h}{\mathrm{d}r}\right)(r-h) - \left(1 + \frac{\mathrm{d}h}{\mathrm{d}r}\right)(r+h)\right\} = 0. \tag{14}$$

It turns out that the function $h = h(r)$ has to vary according to

$$h + r\frac{\mathrm{d}h}{\mathrm{d}r} = 0 \quad \rightarrow \quad h(r) = \frac{c}{r}. \tag{15}$$

By imposing that this transformation must be able to reproduce an ellipse with semiaxis lengths a (along x_1) and b (along x_2) at fixed $r = \bar{r}$, namely that

$$\begin{cases} \left(r - \frac{c}{r}\right)_{r=\bar{r}} = b, \\ \left(r + \frac{c}{r}\right)_{r=\bar{r}} = a, \end{cases} \tag{16}$$

the solution of Eq. (16) is

$$c = \frac{a^2 - b^2}{4}, \qquad \bar{r} = \frac{a+b}{2}, \tag{17}$$

$\bar{r}$ being the average between the semi-axes lengths of the ellipse and c the characteristic feature of the ellipse aspect ratio defined by Eq. (8).

This elliptic-cylindrical mapping, which is similar to the three-dimensional axisymmetric one introduced in Klöcker and Montheillet (1996) to study spheroidal inclusions, is able to describe ellipses characterized by any aspect ratio λ. Hence, separate analyses are not necessary for cylindrical voids with elliptic cross-section of arbitrary aspect ratio $\lambda > 1$ and $\lambda < 1$.

3.1.2. Fully integrated solution of the macroscopic plastic dissipation

In this subsection the orthonormal curvilinear reference frame (13) is used throughout in order to derive an upper bound on the macroscopic yield domain expressed in terms of components of the macroscopic stress tensor, according to the theory of Section 2.

The transformation of coordinates in the RVE transverse cross-section is expressed as

$$\begin{cases} x_1 = r\left(1 - \frac{c}{r^2}\right)\sin\beta, \\ x_2 = r\left(1 + \frac{c}{r^2}\right)\cos\beta, \end{cases} \tag{18}$$

while the absolute value of the Jacobian of this transformation $(r, \beta) \rightarrow (x_1, x_2)$ is given by

$$|J| \equiv \frac{H}{r^3} = \frac{r^4 + c^2 - 2cr^2\cos 2\beta}{r^3}. \tag{19}$$

The computations are developed in what follows under the simplifying assumption that the whole RVE plastically deforms when the macroscopic yield limit is reached. This assumption will be shown in Section 4 to be acceptable, through comparisons with finite element simulations, when the porosity f is not greater than a critical threshold ($f_{\mathrm{E}} \cong 0.2$) at which the load-carrying capacity of the RVE can be assumed to rapidly decay due to the development of localized collapse mechanisms (Koplik and Needleman, 1988).

The components of the continuous velocity field at plastic collapse aligned with the orthonormal reference frame x_1, x_2, x_3 are assumed as follows:

$$\begin{cases} v_1 = X_1(r)x_1 + \dot{E}_{12}x_2, \\ v_2 = \dot{E}_{12}x_1 + X_2(r)x_2, \\ v_3 = \dot{E}_{33}x_3, \end{cases} \tag{20}$$

where the functions $X_1(r)$ and $X_2(r)$ have to be determined. Symmetry of the macroscopic strain rate tensor has been assumed in Eq. (20); the introduction of the uniform shear strain rate field $\dot{E}_{12}$ in the above velocity field allows to take into account the evolution of the orientation of the void axes in the RVE transverse cross-section.

The shear velocity field in Eq. (20) is at variance with respect to that used by Fleck and Hutchinson (1986). In fact, the terms related to $\dot{E}_{12}$ have been deduced here by assuming the velocity field to be curl free,

in order to not introduce a spin at the material level. Further discussions about the effects on the homogenized material properties of the assumed strain rate field can be found in (Corigliano and Mariani, 1998; Mariani, 1998a). Due to the incompressibility of the matrix material, the velocity field (20) must be divergence-free; moreover, it has to satisfy the boundary conditions (2) on ∂V. Relations (20) thus specialize into

$$\begin{cases} v_1 = \frac{1}{2}\left[\frac{a_2 b_2}{r^2 - c}(\dot{E}_a + \dot{E}_{33}) + \dot{E}_b - \frac{2a_2}{a_2 + b_2}\dot{E}_{33}\right]x_1 + \dot{E}_{12}x_2, \\ v_2 = \dot{E}_{12}x_1 + \frac{1}{2}\left[\frac{a_2 b_2}{r^2 + c}(\dot{E}_a + \dot{E}_{33}) - \dot{E}_b - \frac{2b_2}{a_2 + b_2}\dot{E}_{33}\right]x_2, \\ v_3 = \dot{E}_{33}x_3, \end{cases} \tag{21}$$

where

$$\dot{E}_a \equiv \dot{E}_{11} + \dot{E}_{22}, \qquad \dot{E}_b \equiv 2\frac{b_2\dot{E}_{11} - a_2\dot{E}_{22}}{a_2 + b_2}. \tag{22}$$

In the case $\lambda = 1$, i.e., in the case of a circular cylindrical RVE, the component $\dot{E}_a$ is responsible on void size changes at fixed circular void shape whilst the component $\dot{E}_b$ is responsible on void shape changes at fixed void size. As mentioned in Section 2, the velocity field (21) in the RVE does depend on the position vector $\boldsymbol{x}$ in such a way that the microscopic strain rate tensor $\dot{\varepsilon}_{ij}$ differs from the corresponding macroscopic one $\dot{E}_{ij}$.

The velocity field (21) leads, within the framework of J_2-plasticity theory, to the following (square of the) effective microscopic strain rate field:

$$\begin{aligned} \dot{\epsilon}^2_{\mathrm{eq}} &= \frac{2}{3}\left\{\dot{\epsilon}^2_{11} + \dot{\epsilon}^2_{22} + \dot{\epsilon}^2_{33} + 2\dot{\epsilon}^2_{12}\right\} = \frac{2}{3}\left\{\dot{v}^2_{1,1} + \dot{v}^2_{2,2} + \dot{v}^2_{3,3} + \dot{v}^2_{1,2} + \dot{v}^2_{2,1}\right\} \\ &= \frac{1}{3}\left\{\dot{E}_b^2 + 4\left(\ell^2 - \ell + 1\right)\dot{E}^2_{33} + 2(1 - 2\ell)\dot{E}_b\dot{E}_{33} + 4\dot{E}^2_{12} + \frac{a_2 b_2}{H}(\dot{E}_a + \dot{E}_{33})\Big[2\big(r^2\cos 2\beta - c\big)\right. \\ &\qquad \left.\times (\dot{E}_b + (1 - 2\ell)\dot{E}_{33}) + a_2 b_2(\dot{E}_a + \dot{E}_{33}) - 4\dot{E}_{12}r^2\sin 2\beta\Big]\right\} \\ &\equiv \frac{1}{3}\left\{\dot{\Theta}^I_{\mathrm{eq}} + \dot{\Theta}^{II}_{\mathrm{eq}}\cos 2\beta + \dot{\Theta}^{III}_{\mathrm{eq}}\sin 2\beta\right\} \equiv \frac{1}{3}\dot{\Theta}_{\mathrm{eq}}, \end{aligned} \tag{23}$$

where

$$\ell = \frac{a_2}{a_2 + b_2} \tag{24}$$

is a function of the anisotropy (i.e. of the void aspect ratio) in the RVE transverse cross-section and H has been introduced in Eq. (19). In the Eq. (23), a comma means derivative with respect to a coordinate x_i.

According to Eq. (5), the macroscopic plastic dissipation turns out to be expressed as

$$\begin{aligned} \dot{W} = \frac{\sigma_0}{V}\int_\Omega \dot{\epsilon}_{\mathrm{eq}}\,\mathrm{d}\Omega &= \frac{\sigma_0}{\pi L a_2 b_2}\int_0^L \mathrm{d}x_3 \int_{r_1}^{r_2}\frac{1}{r^3}\,\mathrm{d}r\int_0^{2\pi} H\dot{\epsilon}_{\mathrm{eq}}(r,\beta)\,\mathrm{d}\beta \\ &= \frac{\sigma_0}{\sqrt{3}\pi a_2 b_2}\int_{r_1}^{r_2}\frac{1}{r^3}\,\mathrm{d}r\int_0^{2\pi} H\sqrt{\dot{\Theta}_{\mathrm{eq}}}\,\mathrm{d}\beta. \end{aligned} \tag{25}$$

The integration in Eq. (25) is carried out over the volume Ω of the matrix: $\Omega \equiv \{(r,\beta,x_3)\colon r_1 \leqslant r \leqslant r_2, 0 \leqslant \beta \leqslant 2\pi, 0 \leqslant x_3 \leqslant L\}$.

The upper bound on the effective yield domain, here expressed in terms of macroscopic stress components conjugate to the macroscopic strain rates $\dot{E}_a$, $\dot{E}_b$, $\dot{E}_{33}$ and $\dot{E}_{12}$, is obtained as

$$\Sigma_a = \frac{\partial \dot{W}}{\partial \dot{E}_a} = \frac{\sigma_0}{\sqrt{3}\pi a_2 b_2} \int_{r_1}^{r_2} \frac{1}{r^3}\,\mathrm{d}r \int_0^{2\pi} \frac{H\dot{\Theta}_{\mathrm{eq}a}}{2\sqrt{\dot{\Theta}_{\mathrm{eq}}}}\,\mathrm{d}\beta, \tag{26a}$$

$$\Sigma_b = \frac{\partial \dot{W}}{\partial \dot{E}_b} = \frac{\sigma_0}{\sqrt{3}\pi a_2 b_2} \int_{r_1}^{r_2} \frac{1}{r^3}\,\mathrm{d}r \int_0^{2\pi} \frac{H\dot{\Theta}_{\mathrm{eq}b}}{2\sqrt{\dot{\Theta}_{\mathrm{eq}}}}\,\mathrm{d}\beta, \tag{26b}$$

$$\Sigma_{33} = \frac{\partial \dot{W}}{\partial \dot{E}_{33}} = \frac{\sigma_0}{\sqrt{3}\pi a_2 b_2} \int_{r_1}^{r_2} \frac{1}{r^3}\,\mathrm{d}r \int_0^{2\pi} \frac{H\dot{\Theta}_{\mathrm{eq}33}}{2\sqrt{\dot{\Theta}_{\mathrm{eq}}}}\,\mathrm{d}\beta, \tag{26c}$$

$$\Sigma_{12} = \frac{1}{2}\frac{\partial \dot{W}}{\partial \dot{E}_{12}} = \frac{\sigma_0}{2\sqrt{3}\pi a_2 b_2} \int_{r_1}^{r_2} \frac{1}{r^3}\,\mathrm{d}r \int_0^{2\pi} \frac{H\dot{\Theta}_{\mathrm{eq}12}}{2\sqrt{\dot{\Theta}_{\mathrm{eq}}}}\,\mathrm{d}\beta, \tag{26d}$$

where $\dot{\Theta}_{\mathrm{eq}a}$, $\dot{\Theta}_{\mathrm{eq}b}$, $\dot{\Theta}_{\mathrm{eq}33}$ and $\dot{\Theta}_{\mathrm{eq}12}$ are the partial derivatives of $\dot{\Theta}_{\mathrm{eq}}$ with respect to $\dot{E}_a$, $\dot{E}_b$, $\dot{E}_{33}$ and $\dot{E}_{12}$, respectively

$$\dot{\Theta}_{\mathrm{eq}a} \equiv \frac{2a_2b_2}{H}\Big\{a_2b_2(\dot{E}_a+\dot{E}_{33}) + \big(r^2\cos 2\beta - c\big)(\dot{E}_b + (1-2\ell)\dot{E}_{33}) - 2\dot{E}_{12}r^2\sin 2\beta\Big\}, \tag{27a}$$

$$\dot{\Theta}_{\mathrm{eq}b} \equiv \frac{2}{H}\Big\{H[\dot{E}_b + (1-2\ell)\dot{E}_{33}] + a_2b_2(\dot{E}_a+\dot{E}_{33})\big(r^2\cos 2\beta - c\big)\Big\}, \tag{27b}$$

$$\begin{aligned}\dot{\Theta}_{\mathrm{eq}33} \equiv \frac{2}{H}\Big\{H[4\big(\ell^2-\ell+1\big)\dot{E}_{33} + (1-2\ell)\dot{E}_b] + a_2b_2[a_2b_2(\dot{E}_a+\dot{E}_{33}) + \big(r^2\cos 2\beta - c\big)\\ \times(\dot{E}_b + (1-2\ell)(\dot{E}_a+2\dot{E}_{33})) - 2\dot{E}_{12}r^2\sin 2\beta]\Big\},\end{aligned} \tag{27c}$$

$$\dot{\Theta}_{\mathrm{eq}12} \equiv \frac{4}{H}\Big\{2H\dot{E}_{12} - a_2b_2(\dot{E}_a+\dot{E}_{33})r^2\sin 2\beta\Big\}. \tag{27d}$$

The locus of potential yielding can be obtained by varying in the range $]-\infty,\infty[$ the following dimensionless coefficients

$$\varrho = \frac{\dot{E}_a}{\dot{E}_b}, \qquad \vartheta = \frac{\dot{E}_{33}}{\dot{E}_b}, \qquad \chi = \frac{\dot{E}_{12}}{\dot{E}_b}. \tag{28}$$

Notice that $\Sigma_{12} = 0$ when $\chi = 0$ as it can be obtained from Eqs. (26d) and (27d).

The components of the macroscopic stress tensor Σ_{ij} at yielding aligned with the axes of the ellipses in the RVE transverse cross-section are computed according to (Eq. (22))

$$\Sigma_{11} = \frac{\partial \dot{W}}{\partial \dot{E}_{11}} = \frac{\partial \dot{W}}{\partial \dot{E}_a}\frac{\partial \dot{E}_a}{\partial \dot{E}_{11}} + \frac{\partial \dot{W}}{\partial \dot{E}_b}\frac{\partial \dot{E}_b}{\partial \dot{E}_{11}} = \Sigma_a + \frac{2b_2}{a_2+b_2}\Sigma_b, \tag{29a}$$

$$\Sigma_{22} = \frac{\partial \dot{W}}{\partial \dot{E}_{22}} = \frac{\partial \dot{W}}{\partial \dot{E}_a}\frac{\partial \dot{E}_a}{\partial \dot{E}_{22}} + \frac{\partial \dot{W}}{\partial \dot{E}_b}\frac{\partial \dot{E}_b}{\partial \dot{E}_{22}} = \Sigma_a - \frac{2a_2}{a_2+b_2}\Sigma_b, \tag{29b}$$

where use has been made of the chain rule for differentiation.

Under plane strain conditions, that is for $\dot{E}_{33} = 0$, the components of the macroscopic stress tensor at yielding respect the condition (Mariani, 1998b):

$$\Sigma_{33}|_{\vartheta=0} = \frac{\Sigma_{11}|_{\vartheta=0} + \Sigma_{22}|_{\vartheta=0}}{2}. \tag{30}$$

Hence, under plane strain conditions, the relation $\sigma_{33} = (\sigma_{11}+\sigma_{22})/2$, which holds locally for the matrix material, is inherited by the overall yielding property of the RVE.

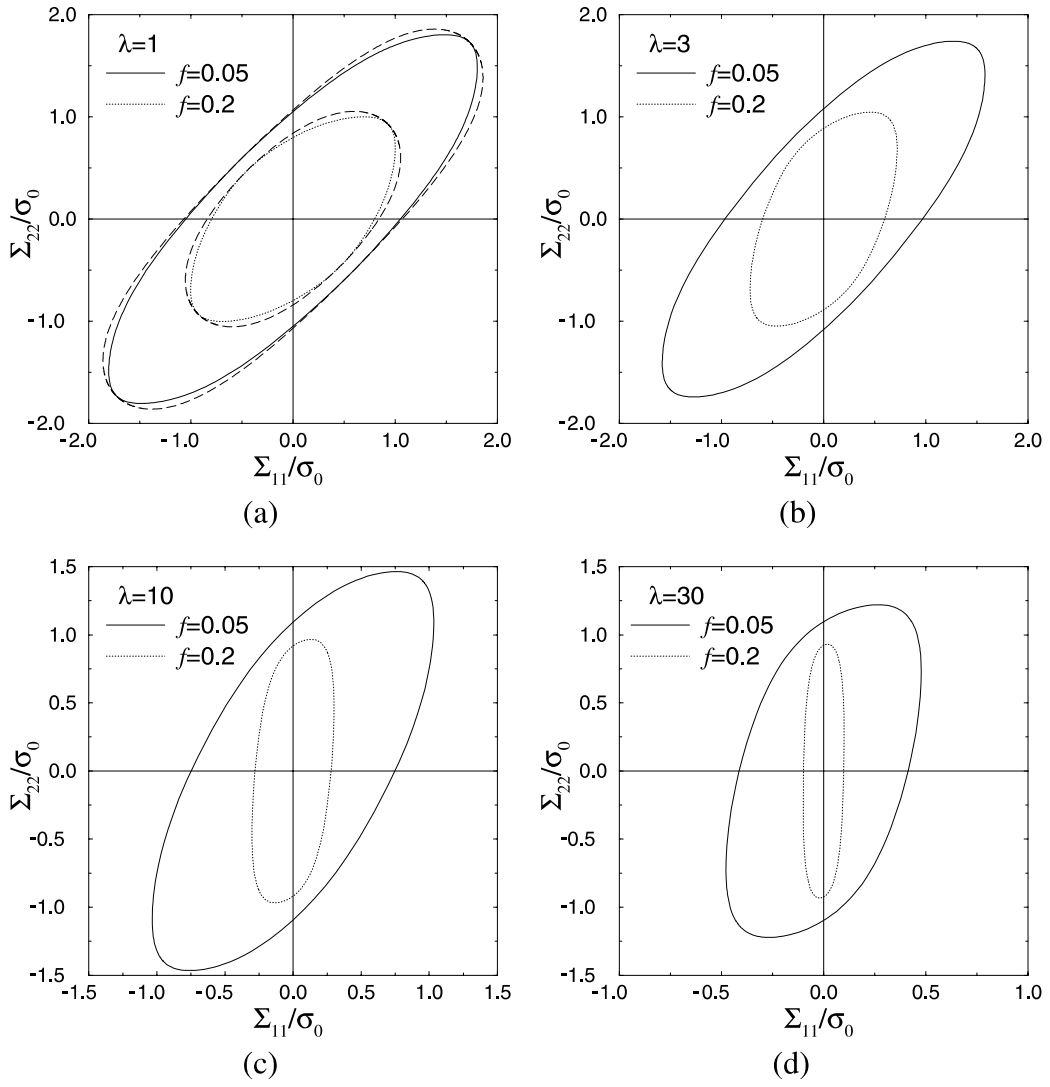

Fig. 2. Effect of the void volume fraction f on the yield surface at fixed void aspect ratios ($\dot{E}_{33} = 0$, $\dot{E}_{12} = 0$): (a) $\lambda = 1$, (b) $\lambda = 3$, (c) $\lambda = 10$, and (d) $\lambda = 30$.

The integration of Eq. (26) has been carried out numerically to obtain the results shown in the following. Under plane strain conditions, Fig. 2 shows the effect of the void volume fraction f on the yield domain at fixed values of void aspect ratio λ and in the absence of the shear strain rate field ($\chi = 0,\ \dot{E}_{12} = 0$). In these plots, the yield domain is represented as projections onto the $\Sigma_{11} - \Sigma_{22}$ plane (recall that $\Sigma_{33} = (\Sigma_{11} + \Sigma_{22})/2$ still holds). The values $f = 0.05, 0.2$ and $\lambda = 1, 3, 10, 30$ have been chosen in order to cover a broad range of porosities and void aspect ratios, that represent material behaviours from the dilutely voided-transversely isotropic case to the mildly voided-orthotropic case. Cases with $\lambda < 1$ ($1/3$, $1/10$, $1/30$), hence with $c < 0$, can be obtained from the same Figs. 2b–d by simply interchanging the Σ_{11} and Σ_{22} components of the macroscopic yield limit. In Fig. 2a, the circular cylindrical Gurson's yield domain has also been drawn with long dashed lines.

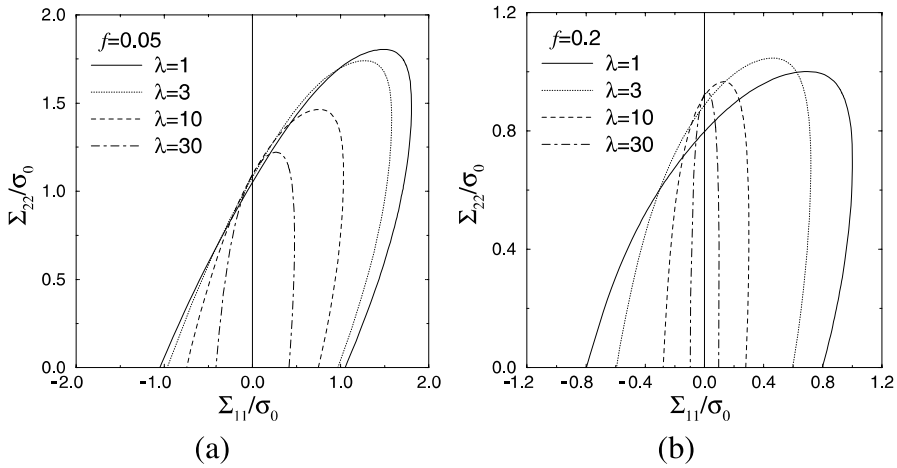

Fig. 3. Effect of the void aspect ratio $\lambda > 1$ on the yield surface at fixed void volume fractions ($\dot{E}_{33} = 0$, $\dot{E}_{12} = 0$): (a) $f = 0.05$, and (b) $f = 0.2$.

In Fig. 3, the influence of the void aspect ratio λ at fixed values of the void volume fraction f is evidenced, again in the absence of the shear strain rate field. Notice that in Fig. 3, the effective yield condition is given only for positive values of the macroscopic stress component Σ_{22} by exploiting the polar symmetry of the overall yield locus with respect to the origin of the $\Sigma_{11} - \Sigma_{22}$ reference frame.

For increasing values of λ, the plots in Figs. 2 and 3 show a stronger reduction of the RVE strength in the x_1 direction, namely along the minor void axis, than in the x_2 direction. At fixed f, an increase of λ

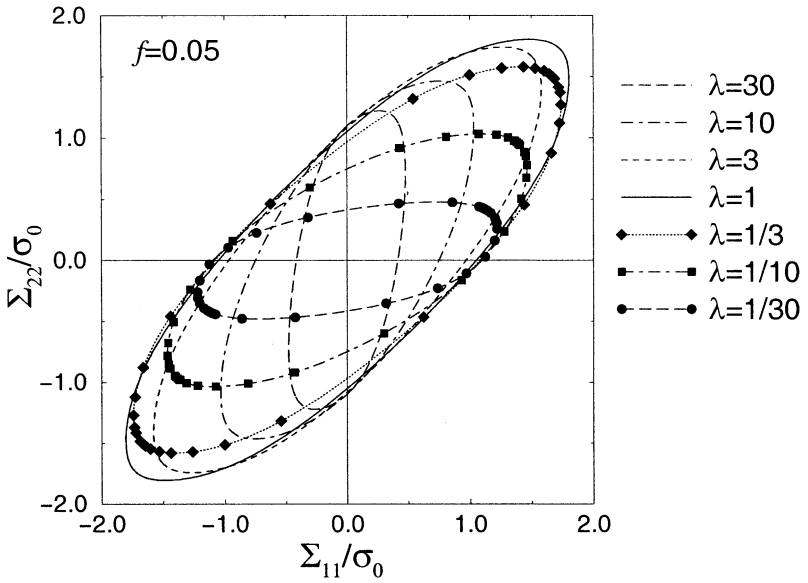

Fig. 4. Effect of the void aspect ratio $\lambda \gtrless 1$ on the yield surface at fixed void volume fraction $f = 0.05$ ($\dot{E}_{33} = 0$, $\dot{E}_{12} = 0$).

causes in fact a considerable reduction in the uniaxial strength along the x_1 direction, represented by the intersection of the macroscopic yield limit with the $\Sigma_{22} = 0$ axis, while a slight increase in the uniaxial strength along the x_2 direction is shown.

In Fig. 4, the macroscopic yield domain is represented at fixed $f = 0.05$ for values of the void aspect ratio $\lambda \geqslant 1$ as well as $\lambda < 1$. The conclusions that void noncircularity acts by destroying the isotropy of the effective yield domain in the $\Sigma_{11} - \Sigma_{22}$ plane and by reducing the maximum stress at yielding for almost any radial path in the $\Sigma_{11} - \Sigma_{22}$ plane can be drawn. Furthermore, Fig. 4 shows that the major reduction in the components of the macroscopic stress tensor at yielding is connected to the direction aligned with the minor axis of the elliptic RVE cross-section.

Fig. 5 concerns the more general situation with $\dot{E}_{12} \neq 0$ and $\Sigma_{12} \neq 0$, still retaining $\dot{E}_{33} = 0$. The yield domain is represented in terms of the three projections onto the $\Sigma_{11} - \Sigma_{12}$, $\Sigma_{22} - \Sigma_{12}$ and $\Sigma_{11} - \Sigma_{22}$ planes. It is worth stressing that also in this case $\Sigma_{33} = (\Sigma_{11} + \Sigma_{22})/2$. For each plane, the influence of the

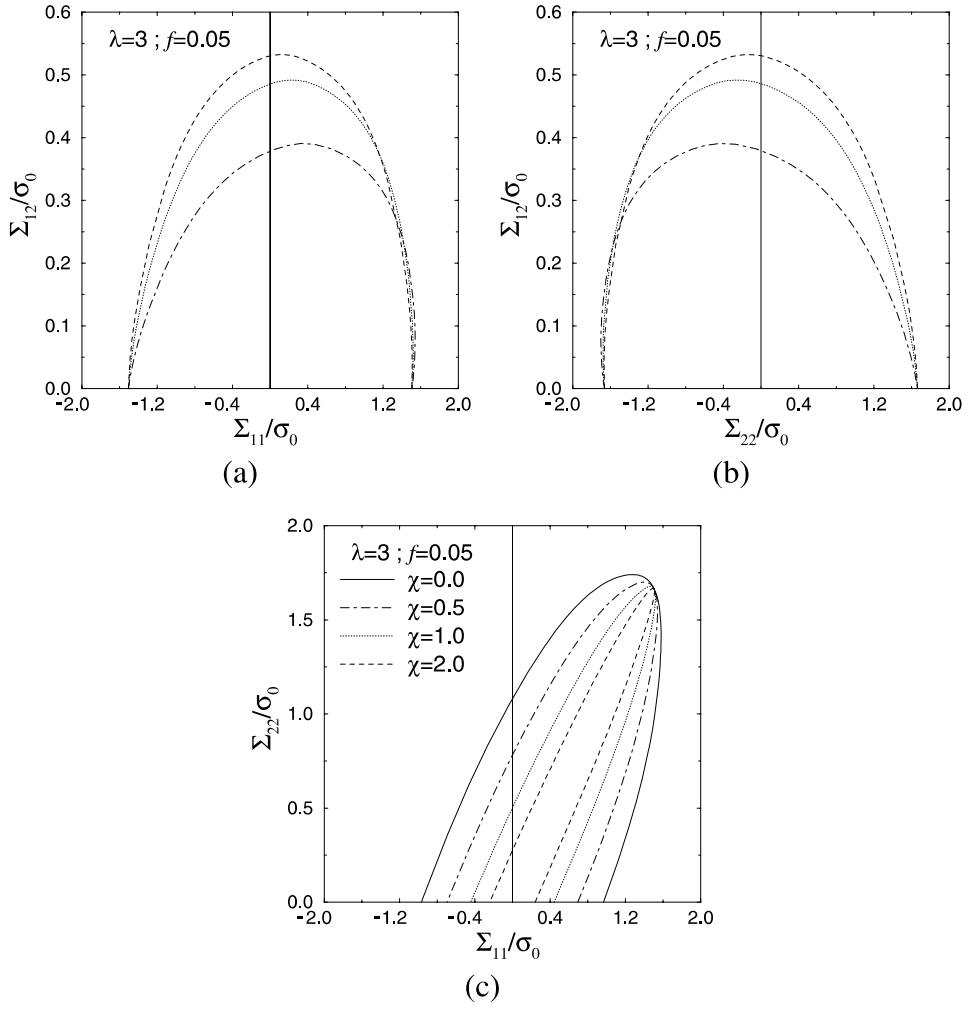

Fig. 5. Effect of the parameter $\chi = \dot{E}_{12}/\dot{E}_b$ on the yield surface at fixed void volume fraction $f = 0.05$ and void aspect ratio $\lambda = 3$ ($\dot{E}_{33} = 0$).

parameter $\chi = \dot{E}_{12}/\dot{E}_b$ on the macroscopic yield domain is shown at fixed $f = 0.05$ and $\lambda = 3$. A reduction of the $\Sigma_{11} - \Sigma_{22}$ projection is related to an increase of the other two $\Sigma_{11} - \Sigma_{12}$ and $\Sigma_{22} - \Sigma_{12}$ projections. In these plots, the effective yield condition is given only for positive values of the macroscopic stress component along the ordinate axis by exploiting again the polar symmetry of the overall yield loci with respect to the origin of the $\Sigma_{11}, \Sigma_{22}, \Sigma_{12}$ reference frame.

From the above figures, it can be noted that both the porosity f and the void aspect ratio λ act as macroscopic *softening* parameters. The introduction of the internal state variable λ in the formulation of a constitutive model for porous, ductile media could, at least partially, reduce the gap between experimental and numerical results concerning localization and fracture phenomena (Tvergaard, 1990). This topic will be treated in details in a companion paper, where a comparison will be presented between results achieved by means of the circular cylindrical Gurson's model with the introduction of the Tvergaard's parameters q_1 and q_2 (Tvergaard, 1981, 1982) and results achieved by means of the newly formulated orthotropic constitutive model.

3.1.3. Approximate solution of the macroscopic plastic dissipation

In order to reduce the computational effort implied in the numerical computation of the effective yield domain through Eq. (26), an approximate solution is here developed.

The approximate yield condition is derived in what follows under the simplifying assumption $\chi = \dot{E}_{12}/\dot{E}_b = 0$ (Eq. (28)) that is in the case of principal directions of the macroscopic strain rate and stress tensors aligned with the axes of the local cartesian orthonormal reference frame x_1, x_2, x_3.

Following the same procedure which leads to the closed-form pressure dependent Gurson's yield condition for circular cylindrical RVE (Gurson, 1977), a Taylor series expansion of the microscopic plastic dissipation in Eq. (25) in terms of $\cos(2\beta)$ is performed about $\cos(2\beta) = 0$. This expansion, if arrested at the first order, gives rise to:

$$\begin{aligned} \dot{W} &= \frac{\sigma_0}{\sqrt{3}\pi a_2 b_2} \int_{r_1}^{r_2} \frac{1}{r^3}\,\mathrm{d}r \int_0^{2\pi} H\sqrt{\dot{\Theta}_{\mathrm{eq}}}\,\mathrm{d}\beta \\ &\cong \frac{2\sigma_0}{\sqrt{3}a_2 b_2} \int_{r_1}^{r_2} \frac{r^4 + c^2}{r^3} \sqrt{\dot{\Theta}^I_{\mathrm{eq}}}\,\mathrm{d}r \equiv \dot{W}^{(0)}, \end{aligned} \tag{31}$$

where $\dot{W}^{(0)}$ stands for the component of $\dot{W}$ associated with the term of zeroth order in $\cos 2\beta$ in the Taylor series expansion and $\dot{\Theta}^I_{\mathrm{eq}}$ has been introduced in Eq. (23). The term $\dot{W}^{(1)}$ is zero being the integral of $\cos 2\beta$ over the domain $[0, 2\pi]$.

The components of the macroscopic stress tensor at yielding can thus be obtained as

$$\Sigma^{(0)}_a = \frac{\partial \dot{W}^{(0)}}{\partial \dot{E}_a} = \frac{2\sigma_0}{\sqrt{3}a_2 b_2} \int_{r_1}^{r_2} \frac{r^4 + c^2}{r^3} \frac{\dot{\Theta}^I_{\mathrm{eq}a}}{2\sqrt{\dot{\Theta}^I_{\mathrm{eq}}}}\,\mathrm{d}r, \tag{32a}$$

$$\Sigma^{(0)}_b = \frac{\partial \dot{W}^{(0)}}{\partial \dot{E}_b} = \frac{2\sigma_0}{\sqrt{3}a_2 b_2} \int_{r_1}^{r_2} \frac{r^4 + c^2}{r^3} \frac{\dot{\Theta}^I_{\mathrm{eq}b}}{2\sqrt{\dot{\Theta}^I_{\mathrm{eq}}}}\,\mathrm{d}r, \tag{32b}$$

$$\Sigma^{(0)}_{33} = \frac{\partial \dot{W}^{(0)}}{\partial \dot{E}_{33}} = \frac{2\sigma_0}{\sqrt{3}a_2 b_2} \int_{r_1}^{r_2} \frac{r^4 + c^2}{r^3} \frac{\dot{\Theta}^I_{\mathrm{eq}33}}{2\sqrt{\dot{\Theta}^I_{\mathrm{eq}}}}\,\mathrm{d}r, \tag{32c}$$

where

$$\dot{\Theta}^I_{\mathrm{eq}a} \equiv \frac{2a_2b_2}{r^4+c^2}\Big\{a_2b_2(\dot{E}_a+\dot{E}_{33})-c(\dot{E}_b+(1-2\ell)\dot{E}_{33})\Big\}, \tag{33a}$$

$$\dot{\Theta}^I_{\mathrm{eq}b} \equiv \frac{2}{r^4+c^2}\Big\{(r^4+c^2)(\dot{E}_b+(1-2\ell)\dot{E}_{33})-a_2b_2(\dot{E}_a+\dot{E}_{33})c\Big\}, \tag{33b}$$

$$\dot{\Theta}^I_{\mathrm{eq}33} \equiv \frac{2}{r^4+c^2}\Big\{(r^4+c^2)(4(\ell^2-\ell+1)\dot{E}_{33}+(1-2\ell)\dot{E}_b)+a_2b_2[a_2b_2(\dot{E}_a+\dot{E}_{33}) - c(\dot{E}_b+(1-2\ell)(\dot{E}_a+2\dot{E}_{33}))]\Big\}. \tag{33c}$$

Eq. (32) can be analytically expressed in terms of elliptic integrals of the first and second kinds. These integrals play a special role in several fields of applied mathematics and fast algorithms are available for their numerical computation (Press et al., 1992); topics related to the numerical integration of Eq. (32) is not treated here for brevity.

Under plane strain conditions, a comparison between the yield locus obtained by means of the numerical computation of integrals (26) for $\dot{E}_{33}=0$ and by means of the semi-analytical integration of the approximate solution (32) is shown in Fig. 6 for $\lambda=3$ and $\lambda=30$. The solution for $\lambda=1$ has been previously depicted in Fig. 2a: the approximate solution here proposed, in fact, matches for $\lambda=1$, the analytical original formulation given by Gurson for a transversely isotropic circular cylindrical RVE (Gurson, 1977). Long-dashed curves in Fig. 2a represent the analytical approximate yield domain, which is an upper bound on the exact solution for the homogenized yield condition as computed according to the theory revised in Section 2.

Analogous conclusions can be stated for orthotropic solids (Fig. 6): approximation (32) constitutes an upper bound on the solution (26) of the problem. The degree of accuracy of the current yield domain with respect to the exact solution is thus reduced by the simplifications introduced in order to obtain an analytical (or semi-analytical) description of the plastic behaviour of porous solids. Furthermore, from Figs. 2a and 6, the effects of f and λ on the approximations introduced by Eq. (32) can be appreciated. As a general trend, the accuracy of the numerical solution is progressively reduced in an average way by increasing values of f and λ. The plots show that the difference between the two solutions also depends on the path followed in the plane $\Sigma_{11}-\Sigma_{22}$ of the macroscopic stress components: for stress states that predominantly evolve along the Σ_{22} axis, no differences are shown between exact and approximate yield limits; on the other hand, for stress states which are mainly characterized in terms of the Σ_{11} component, a more pronounced scatter exists between the exact solution and the approximate one.

As far as three-dimensional (3D) loading conditions are concerned, at fixed value of porosity $f=0.05$, the effective yield locus is shown in Figs. 7 and 8 for $\lambda=1$ and $\lambda=30$, respectively. These 3D yield domains are given in terms of projections onto the $\Sigma_{11}-\Sigma_{33}$, $\Sigma_{22}-\Sigma_{33}$ and $\Sigma_{11}-\Sigma_{22}$ macroscopic stress planes. The domains are represented in these plots by means of meridians through their poles and by means of parallels to the equator. Specifically, the poles of the yield domain are the points characterized by the maximum distance from the origin of the $\Sigma_{11},\Sigma_{22},\Sigma_{33}$ reference frame, and the equator is the intersection between the yield domain and a plane whose unit normal vector has the same direction of the line through the poles.

As for the yield domain obtained by the fully integrated solution of the macroscopic plastic dissipation, the aspect ratio λ acts by progressively reducing the dimensions of the effective yield surface. This noteworthy reduction of the effective yield domain with respect to the transversely isotropic Gurson's one represented in Fig. 7 is accompanied by a rotation of the line through the poles of the domain. In particular, this rotation highly affects the projections onto the $\Sigma_{11}-\Sigma_{33}$ and $\Sigma_{11}-\Sigma_{22}$ planes, whilst the direction cosines of the line through the poles in the Σ_{22} and Σ_{33} directions are not affected much. This aspect is a manifestation of what is already shown by Figs. 2 and 3: the major reduction in the homogenized strength properties of the elliptic-cylindrical RVE is displayed along the reference axis x_1 that is along the minor principal axis of the elliptic void cross-section.

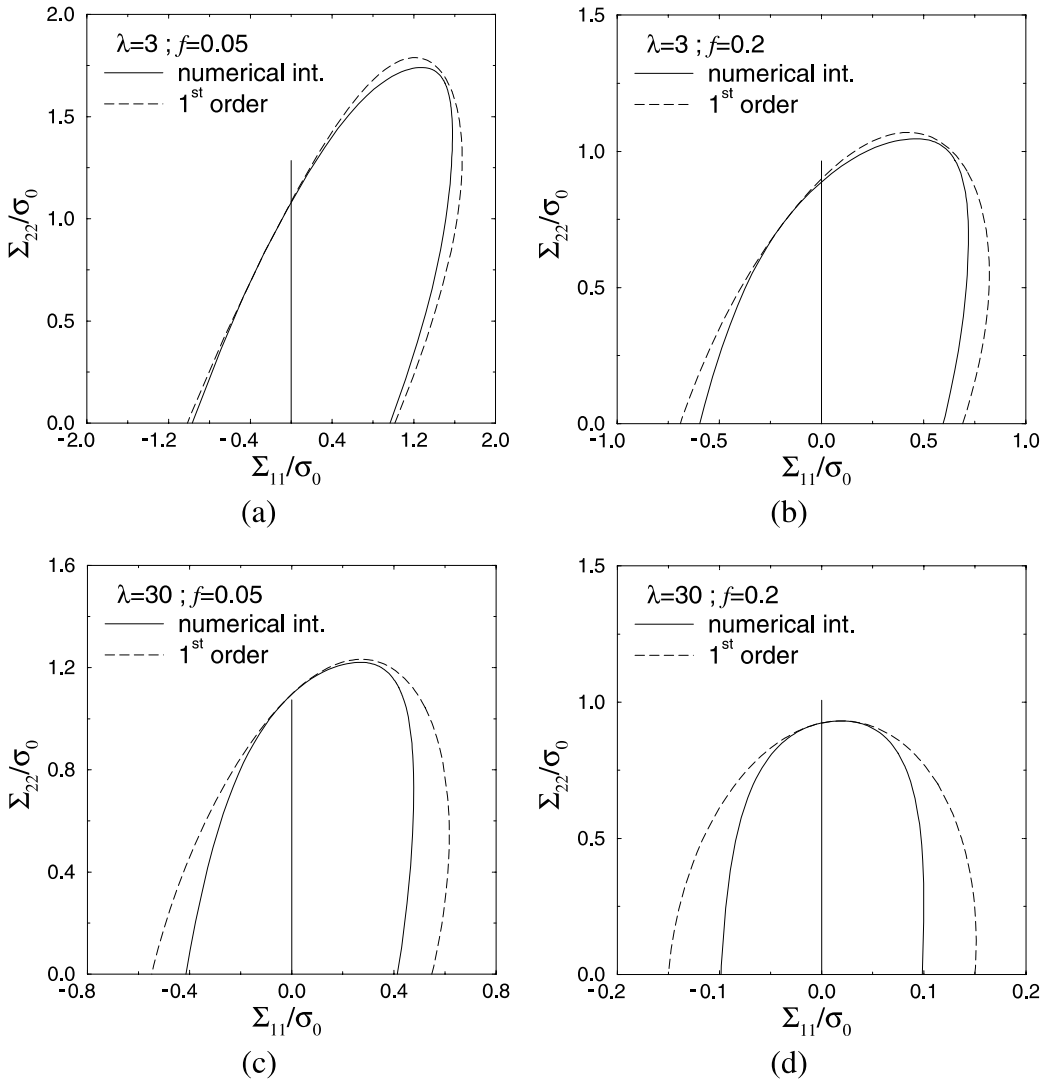

Fig. 6. Comparison between analytical solution and approximate estimation of the yield surface ($\dot{E}_{33} = 0$, $\dot{E}_{12} = 0$): (a) $f = 0.05$, $\lambda = 3$; (b) $f = 0.2$, $\lambda = 3$; (c) $f = 0.05$, $\lambda = 30$; and (d) $f = 0.2$, $\lambda = 30$.

3.2. Evolution laws for the void volume fraction and aspect ratio

The orthotropic model here developed is able to take into account the anisotropy in the RVE transverse cross-section, at difference with respect to the original circular cylindrical Gurson's model.

This anisotropy can be due to the shape of the inclusions at the beginning of the deformation process as generated during metal forming processes like, e.g., rolling. In such a case, the orientation of the inclusions is not randomly distributed; the isotropy or transverse isotropy is thus lost and privileged material directions must be taken into account. The anisotropy can also be induced by plastic straining for initially transversely isotropic inclusion shapes and spatial distributions.

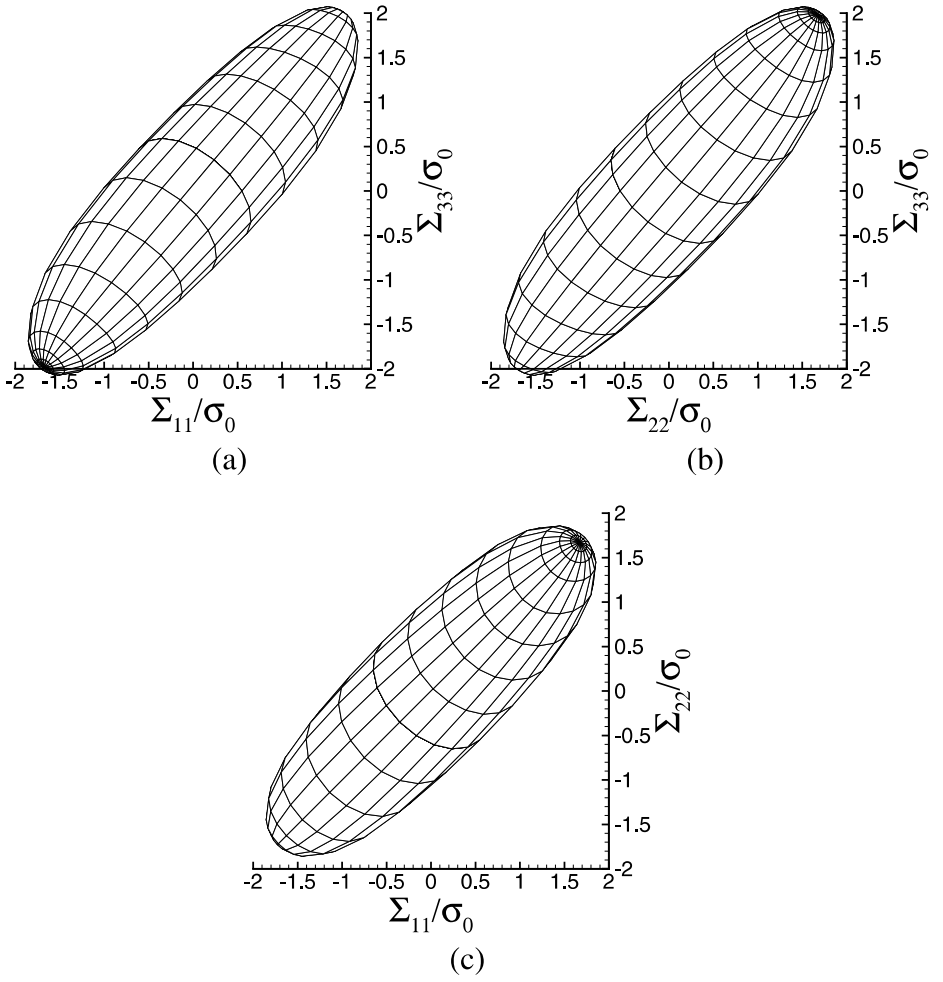

Fig. 7. Projections onto the (a) $\Sigma_{11} - \Sigma_{33}$, (b) $\Sigma_{22} - \Sigma_{33}$ and (c) $\Sigma_{11} - \Sigma_{22}$ planes of the 3D effective yield condition of orthotropic porous solid for $f = 0.05$, $\lambda = 1$ ($\dot{E}_{12} = 0$).

By neglecting the effects of the induced anisotropy during the loading process, the material strength is overestimated as it can be seen from the smaller dimensions of the effective yield domains (represented in Figs. 7 and 8 in terms of the stress components $\Sigma_{11}, \Sigma_{22}, \Sigma_{33}$ at yielding) at higher values of λ for a fixed value of porosity f.

The development of upper bounds on the effective yield loci for orthotropic porous media thus requires a more refined description of the microstructure evolution, due to the strong dependence of the results on the void size and shape.

In this subsection, results concerning microstructure evolution are presented in the absence of a shear strain rate field in the RVE cross-section related to $\dot{E}_{12}$. For principal directions of the macroscopic strain rate and stress tensors aligned with the axes of the cartesian reference frame x_1, x_2, x_3, namely with the privileged directions of the RVE geometry, the microstructure is completely defined through the void volume fraction f and the void aspect ratio λ; the void orientation with respect to a fixed global reference frame is maintained fixed throughout the whole deformation process.

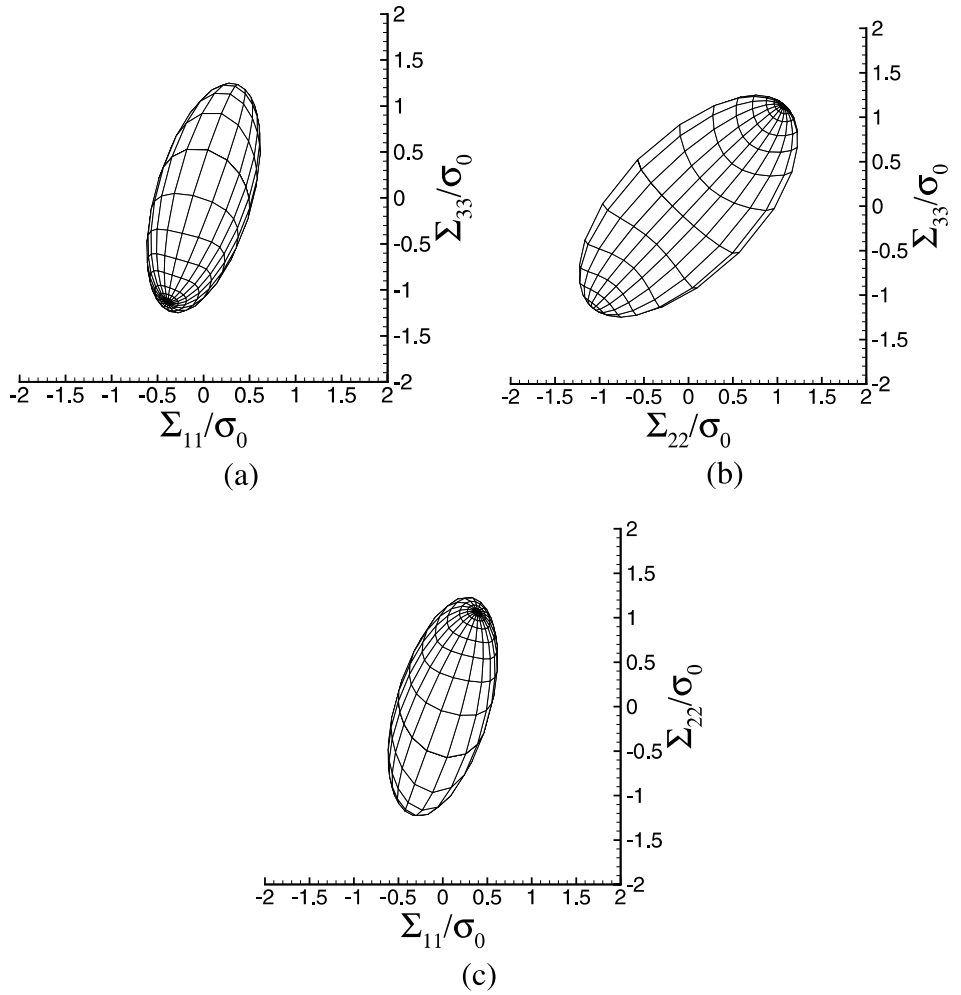

Fig. 8. Projections onto the (a) $\Sigma_{11} - \Sigma_{33}$, (b) $\Sigma_{22} - \Sigma_{33}$ and (c) $\Sigma_{11} - \Sigma_{22}$ planes of the 3D effective yield condition of orthotropic porous solid for $f = 0.05$, $\lambda = 30$ ($\dot{E}_{12} = 0$).

Furthermore, it can be shown that the velocity field (21) allows the void to evolve maintaining an elliptic cross-section.

By exploiting the matrix incompressibility, the evolution laws for the porosity f and the void aspect ratio λ can be computed as

$$\dot{f} = \left(\frac{\dot{V}_v}{V}\right)^{\cdot} = (1-f)\frac{\dot{V}_v}{V} = (1-f)\dot{E}_{kk}, \tag{34}$$

$$\dot{\lambda} = \left(\frac{a_1}{b_1}\right)^{\cdot} = \frac{\lambda}{f}\frac{1-\lambda}{1+\lambda}\dot{E}_{kk} - \lambda\dot{E}_b - \lambda\frac{1-\kappa_v}{1+\kappa_v}\dot{E}_{33}, \tag{35}$$

where parameter κ_v has been defined in Eq. (12) and $\dot{E}_{kk}$ is the trace of the macroscopic strain rate tensor ($\dot{E}_{kk}$ can generally differ from zero due to the macroscopic dilatant behaviour).

This orthotropic constitutive model for porous, ductile media thus represents a generalization of the original Gurson's model for transversely isotropic porous solids and is related to a more refined description of the microstructure and of the microstructure evolution. In the preceding analysis, it has been assumed that the RVE geometry is characterized by two confocal ellipses, which are the void-matrix interface and the longitudinal RVE outer boundary. Nevertheless, the velocity field (21) causes the two ellipses to have different foci at the end of the rate deformation process: this means that an approximation has been introduced in the model in order to obtain the analytical results developed here.

4. Unit cell finite element simulations

In Section 3, approximate upper bounds on the effective yield loci for orthotropic porous, ductile media have been obtained. In order to check their degree of accuracy and to quantify the overestimation of the modelled overall strength, finite element (FE) simulations concerning the single RVE are here presented.

A spatial discretization of the RVE geometry is introduced by means of finite elements; loading conditions are imposed on the external surface of the FE aggregate according to Eq. (2), while tractions-free conditions are applied at the interface between the void and the matrix.

The results discussed hereafter concern only the RVE strength under monotonically increasing radial paths in the space of the macroscopic strain-rate tensor components. The final plastic collapse of the RVE (for assumed linearized kinematics) is identified by the formation of local mechanisms within the matrix volume.

The degree of accuracy of the theoretical results is mainly connected to the capacity of the applied loading conditions to develop a collapse mechanism that spreads over almost the whole matrix volume. In fact, it has been assumed in the analytical derivation that the microscopic strain rate fields are continuous functions within the rigid ideally plastic matrix.

The FE meshes used are different from those usually employed to check the transferability of Gurson's model at the material level. Here, the RVE geometry discretized by FEs is exactly the same as that used for the analytical solution of the homogenization problem. In other works (Koplik and Needleman, 1988; Needleman, 1972; Hom and McMeeking, 1989; Guennouni and Francois, 1987; Becker et al., 1989; Brocks, 1995; Tvergaard, 1997), the unit cell geometry represents a real volume element, which is able to reproduce the whole continuum without gaps or overlaps. This difference is due to the fact that aim of this section is to appraise the approximations introduced in the analytical treatment of the problem.

In order to simplify the geometry and the assessment of the dissipation mechanisms in the matrix material during the analyses, the results are presented in what follows for the two-dimensional plane strain case. The FE meshes are composed by plane strain, four-node B-bar elements, whose edges are disposed along lines at $r = \text{constant}$ and $\beta = \text{constant}$ (Figs. 10 and 11). The matrix material obeys an (elastic) ideally plastic J_2-flow theory of plasticity. Results are presented in terms of components of the macroscopic stress tensor Σ_{ij} at yielding, which are computed according to their definition (1) as the volume averages of the relevant local stress components σ_{ij}. By imposing external loading conditions at varying $\varrho \equiv \dot{E}_a/\dot{E}_b$ and $\chi \equiv \dot{E}_{12}/\dot{E}_b$, a set of points of the yield domain are obtained for the corresponding radial strain-rate paths.

Fig. 9 shows results concerning load cases with $\chi = \dot{E}_{12}/\dot{E}_b = 0$ (no shear) and a comparison with the analytical findings (numerical integration of Eq. 26). In this case, due to the symmetry, only one quarter of the cross-section of the cylindrical RVE has been analyzed.

As can be seen from Fig. 9, the agreement between FE and theoretical results is good, specially for the lower values of porosity f and aspect ratio λ. The distance between the theoretical upper bound and the FE results increases at increasing values of void aspect ratio λ. In the case of $\lambda = 10$, the theoretical results strongly overestimate the RVE strength in the x_1 direction. This fact can be justified by examining the contour plots of the dimensionless effective stress within the matrix, drawn in Figs. 10 and 11, which

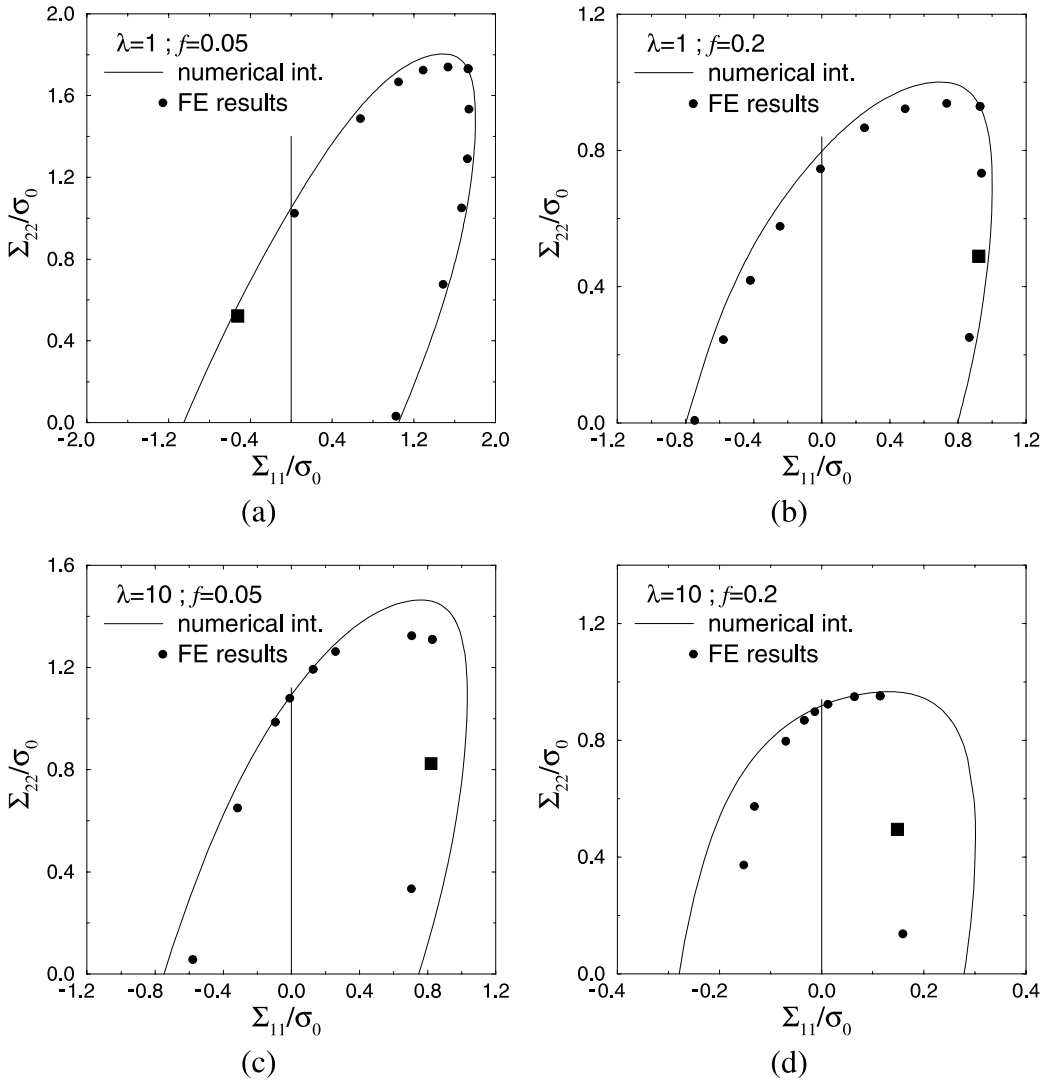

Fig. 9. Comparison between analytical solution and FE results ($\dot{E}_{33} = 0$, $\dot{E}_{12} = 0$): (a) $f = 0.05$, $\lambda = 1$; (b) $f = 0.2$, $\lambda = 1$; (c) $f = 0.05$, $\lambda = 10$; and (d) $f = 0.2$, $\lambda = 10$.

correspond to limit situations marked with squared symbols in Figs. 9c and d, respectively. As can be appreciated from the contour plots, the plastic collapse mechanism is partial; in the region(s) where $\sigma_{eq}/\sigma_0 < 1$ (colored with lighter grey levels in the figures), the yield limit is not reached and the material does not deform plastically. This feature is in contrast with the hyphotesis of fully plastic situation within the matrix volume at the basis of the theoretical analysis.

In Fig. 12, the results concerning the loading case with $\chi = \dot{E}_{12}/\dot{E}_b = 1$ (shear) are shown. The whole RVE cross-section has been discretized by FEs in this case. The same remarks done with reference to the shear-free loading conditions hold. In addition, it can be observed from Fig. 12c that some points obtained with FE computations seem to be slightly outside the theoretical upper bound on the yield domain. This is a graphical effect caused by the projection of the results onto the $\Sigma_{11} - \Sigma_{22}$ plane. A comparison made on the

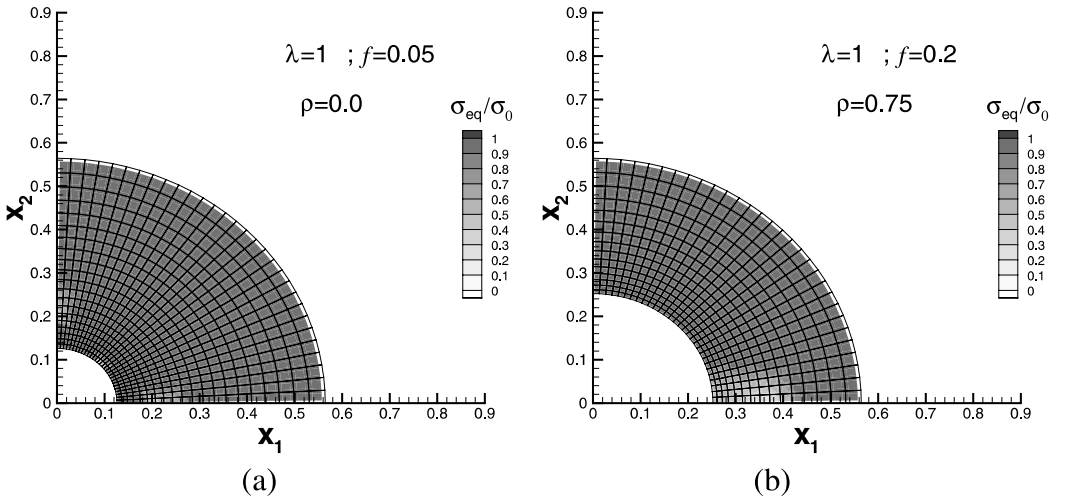

Fig. 10. Computed dimensionless effective stress fields in the matrix material for $\lambda = 1$ ($\dot{E}_{33} = 0$, $\dot{E}_{12} = 0$): (a) $f = 0.05$, and (b) $f = 0.2$.

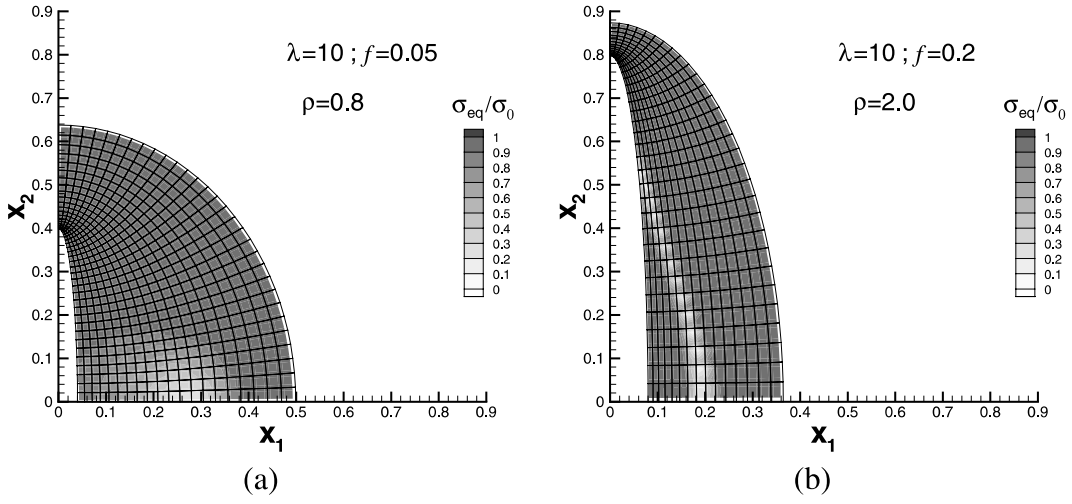

Fig. 11. Computed dimensionless effective stress fields in the matrix material for $\lambda = 10$ ($\dot{E}_{33} = 0$, $\dot{E}_{12} = 0$): (a) $f = 0.05$, and (b) $f = 0.2$.

norm of the stress tensor at yielding, as obtained from analytical results and FE simulations, shows that the analytical results constitute a real upper bound on the effective yield locus, even in the presence of shear strain rate loading conditions.

5. Discussion and closing remarks

The present paper mainly focused on the development of macroscopic yield conditions for anisotropic porous, ductile media.

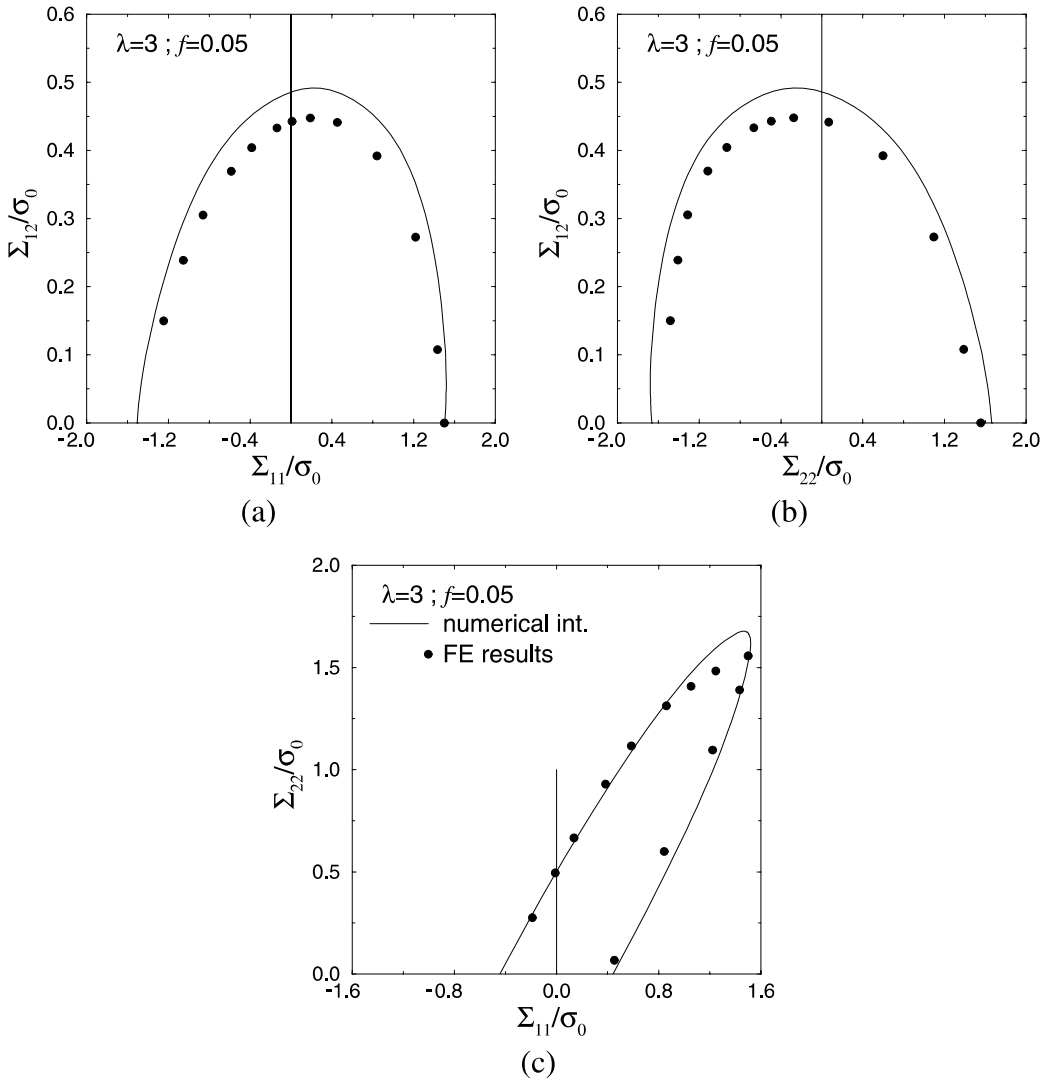

Fig. 12. Comparison between analytical solution and FE results for $f = 0.05$, $\lambda = 3$ ($\dot{E}_{33} = 0$, $\dot{E}_{12} \neq 0$).

The approach originally proposed by Gurson to obtain his constitutive model has been chosen in order to derive upper bounds on the macroscopic yield conditions for cylindrical RVE with an elliptic cross-section containing a coaxial and confocal elliptic-cylindrical cavity. Analytical developments as well as approximate solutions have been presented with different degrees of approximation.

Besides the porosity, the void aspect ratio appears as a further internal state variable, which influences the macroscopic yield domain. The evolution laws for the internal state variables have been explicitly obtained.

The analytical results in terms of macroscopic yield domains have been finally compared with finite element simulations.

To the authors' knowledge, the paper contains a number of analytical results which contribute in the understanding of the micromechanics of ductile fracture processes. These can be listed as follows:

- The influence of void aspect ratio on the macroscopic yield domain has been explicitly put in evidence. It appears clearly that void aspect ratio can act as a softening variable which strongly reduces the strength of the RVE.
- While the evolution law for the void volume fraction f can be simply derived from the conservation of mass principle, the evolution law for the void aspect ratio λ shows a complicate dependence on the loading conditions (through the components of the macroscopic strain rate tensor) and on the current microstructure (through the current values of f and λ).
- Analytical results have been obtained under the assumption of continuous strain rate fields within the rigid ideally plastic matrix material. From a comparison with finite element simulations of plastic collapse mechanisms under the same loading conditions, discontinuous strain rate fields seem to develop in the matrix, thus leading to possible enhanced conditions for localization of plastic deformations in preferred *weak* bands. This phenomena can give rise to a consistent reduction of the RVE strength properties with respect to the analytical results even during the void growth process, under strain levels and for porosity values below the thresholds at which void coalescence mechanisms take place.

The above results represent the first part of a study aiming at the development and numerical implementation of a constitutive model for porous, ductile materials which takes into account the anisotropy arising at the microscale. The macroscopic yield domain and the evolution laws of the internal state variables presented in this paper can be directly used in the formulation of an elastoplastic constitutive model at the macroscopic level. A particular aspect which arises from this theory is that the macroscopic yield domain for porous media with orthotropic microstructure is expressed in a parametric way.

The following issues, which are particularly worth being addressed to the authors' opinion, are now being considered or will be considered in the next future:

- improvement of the upper bounds on the macroscopic yield condition through the introduction of discontinuous local plastic strain rate fields,
- formulation of an analytical lower bound on the macroscopic yield condition,
- generalization of the obtained results by allowing the principal axes of loading to be different from the principal axes of the elliptic cross-section geometry. In this case, the evolution of the ellipse axes orientation must be considered in the formulation.

Acknowledgements

This paper has been carried out in the framework of the project PF MSTA II contract No. 97.00906.PF34, financed by CNR (Italian National Research Council).

References

Becker, R., Smelser, R.E., Richmond, O., Appleby, E.J., 1989. The effect of void shape on void growth and ductility in axisymmetric tension tests. Metallurgical Transactions 20A, 853–861.

Bishop, J.F.W., Hill, R., 1951. A theory of the plastic distorsion of a polycrystalline aggregate under combined stresses. Philosophical Magazine 42, 414–427.

Brocks, W., Sun, D.-Z., Honig, A., 1995. Verification of the transferability of micromechanical parameters by cell model calculations with visco-plastic materials. International Journal of Plasticity 11, 971–989.

Chu, C.C., Needleman, A., 1980. Void nucleation effects in biaxially stretched sheets. ASME Journal of Engineering Materials and Technology 102, 249–256.

Corigliano, A., Mariani, S., 1998. Constitutive models for metals containing non-spherical voids. In: Idelsohn, S.R., Oñate, E., Dvorkin, E.N. (Eds.), Proceedings of the Fourth World Congress on Computational Mechanics, Buenos Aires, Argentina.

Faleskog, J., Shih, C.F., 1997. Micromechanics of coalescence-I. Synergistic effects of elasticity, plastic yielding and multi-size-scale voids. Journal of the Mechanics and Physics of Solids 45, 21–50.

Fleck, N.A., Hutchinson, J.W., 1986. Void growth in shear. Proceedings of the Royal Society of London A407, 435–458.

Gologanu, M., Leblond, J.-P., Devaux, J., 1993. Approximate models for ductile metals containing non-spherical voids – case of axisymmetric prolate ellipsoidal cavities. Journal of the Mechanics and Physics of Solids 41, 1723–1754.

Gologanu, M., Leblond, J.-P., Devaux, J., 1994. Approximate models for ductile metals containing non-spherical voids – case of axisymmetric oblate ellipsoidal cavities. ASME Journal of Engineering Materials and Technology 116, 290–297.

Goods, S.H., Brown, L.M., 1979. The nucleation of cavities by plastic deformation. Acta Metallurgica 27, 1–15.

Guennouni, T., Francois, D., 1987. Constitutive equations for rigid plastic or viscoplastic materials containing voids. Fatigue and Fracture of Engineering Materials and Structures 10, 399–418.

Gurson, A.L., 1977. Continuum theory of ductile rupture by void nucleation and growth: Part I. Yield criteria and flow rules for porous ductile media. ASME Journal of Engineering Materials and Technology 99, 2–15.

Hom, C.L., McMeeking, R.M., 1989. Void growth in elastic–plastic materials. ASME Journal of Applied Mechanics 56, 309–317.

Kailasam, M., Castañeda, P.P., Willis, J.R., 1997a. The effect of particle size, shape, distribution and their evolution on the constitutive response of nonlinear viscous composites. I. Theory. Philosophical Transactions of the Royal Society of London A 355, 1835–1852.

Kailasam, M., Castañeda, P.P., 1997b. The effect of particle size, shape, distribution and their evolution on the constitutive response of nonlinear viscous composites. II. Examples. Philosophical Transactions of the Royal Society of London A 355, 1853–1872.

Kailasam, M., Castañeda, P.P., 1998. A general constitutive theory for linear and nonlinear particulate media with microstructure evolution. Journal of the Mechanics and Physics of Solids 46, 427–465.

Klöcker, H., Montheillet, F., 1996. Velocity, strain rate and stress fields around a spheroidal cavity in a linearly viscous material. European Journal of Mechanics A/Solids 15, 397–422.

Koplik, J., Needleman, A., 1988. Void growth and coalescence in porous plastic solids. International Journal of Solids and Structures 24, 835–853.

Lee, B.J., Mear, M.E., 1991. On the yield strength of metals containing spheroidal inclusions or voids. Mechanics of Materials 12, 191–205.

Lee, B.J., Mear, M.E., 1992a. Axisymmetric deformation of power-law solids containing a dilute concentration of aligned spheroidal voids. Journal of the Mechanics and Physics of Solids 40, 1805–1836.

Lee, B.J., Mear, M.E., 1992b. Effective properties of power-law solids containing elliptical inhomogeneities. Part I: Rigid inclusions. Mechanics of Materials 13, 313–335.

Lee, B.J., Mear, M.E., 1992c. Effective properties of power-law solids containing elliptical inhomogeneities. Part II: Voids. Mechanics of Materials 13, 337–356.

Lemaitre J, 1992. A Course on Damage Mechanics. Springer, Berlin.

Maier, G., Drucker, D.C., 1973. Effects on geometry change on essential features of inelastic behaviour. ASCE Journal of the Engineering Mechanics Division 99, 819–834.

Malvern, L.E., 1969. Introduction to the Mechanics of a Continuous Medium Prentice-Hall, N.J.

Mariani, S., 1998a. An anisotropic constitutive model for void-containing ductile solids. In: Sglavo V.M. (Ed.), Proceedings of the XIV Congress of the Italian Group of Fracture, Italy, pp. 331–338.

Mariani, S., 1998b. Simulation of ductile fracture: material models, computational aspects and parameter identifications Ph.D Thesis, Politecnico di Milano.

McClintock, F.A., 1968. A criterion for ductile fracture by the growth of holes. ASME Journal of Applied Mechanics 35, 363–371.

Needleman, A., 1972. Void growth in a elastic-plastic medium. ASME Journal of Applied Mechanics 41, 964–970.

Castañeda, P.P., Zaidman, M., 1994. Constitutive models for porous materials with evolving microstructure. Journal of the Mechanics and Physics of Solids 42, 1459–1497.

Castañeda, P.P., 1996. Nonlinear composite materials: effective constitutive behaviour and microstructure evolution. In: Suquet, P. (Ed.) Continuum micromechanics, CISM Courses and Lectures, Springer, Berlin, pp. 131–195.

Press, W.H., Teukolsky, S.A., Vetterling, W.T., Flannery, B.P., 1992. Numerical recipes in Fortran. The art of scientific computing , second ed. Cambridge University Press.

Rousselier, G., Finite deformation constitutive relations including ductile fracture damage. In: Nemat-Nasser, S. (Ed.), Three-dimensional Constitutive Relations and Ductile Fracture, North-Holland Publishing, pp. 331–355.

Rice, J.R., Tracey, D.M., 1969. On the ductile enlargement of voids in triaxial stress field. Journal of the Mechanics and Physics of Solids 17, 201–217.

Speich, G.R., Spitzig, W.A., 1982. Effect of volume fraction and shape of sulfide inclusions on through-thickness ductility and impact energy of high-strength 4340 plate steels. Metallurgical Transactions 13A, 2239–2258.

Suquet, P., 1996. Effective properties of nonlinear composites. In: Suquet, P. (Ed.), Continnum Micromechanics, CISM Courses and Lectures, Springer, Berlin, pp. 197-264.

Taliercio, A., 1992. Lower and upper bounds to the microscopic strenght domain of a fiber-reinforced composite material. International Journal of Plasticity 8, 741–762.

Tvergaard, V., 1981. Influence of voids on shear band instabilities under plane strain conditions. International Journal of Fracture 17, 389–407.

Tvergaard, V., 1982. Ductile fracture by cavity nucleation between larger voids. Journal of the Mechanics and Physics of Solids 30, 265–286.

Tvergaard, V., 1990. Material failure by void growth to coalescence. Advances in applied Mechanics 27, 83–151.

Tvergaard, V., 1997. Studies of void growth in a thin ductile layer between ceramics. Computational Mechanics 20, 186–191.

Xia, L., Shih, C.F., Hutchinson, J.W., 1995. A computational approach to ductile crack growth under large scale yielding conditions. Journal of the Mechanics and Physics of Solids 43, 389–413.

Yee, K.C., Mear, M.E., 1996. Effect of void shape on the macroscopic response of non-linear porous solids. International Journal of Plasticity 12, 45–68.